Experimental Study of Hydrogen Production Using Electrolysis Process Powered by Wind and Solar Energy

Faisal Rahman, M.S.K. Tony Suryo Utomo, Berkah Fajar T.K.

Abstract— One of the alternative energy storage media that is predicted to be the energy of the future as an effort to shift the energy production from conventional energy to renewable energy is hydrogen, due to its adequate energy content with high heating value (HHV) of 141 MJ/kg and several other properties that make it suitable for use as an energy storage medium. 95% of hydrogen gas production is currently dominated by fossil-based process. In this research, experiment will be carried out to produce hydrogen gas based on renewable energy using wind turbine and solar panels. The goal of combining these two energy sources is to complement each other's intermittent nature of each energy source. This experiment uses alkaline water electrolysis process with 30 wt% NaOH solution as the electrolyte and 316 L stainless steel as the electrode material used in the electrolyzer. The main objective of this study is to determine the overall system efficiency, electrolysis efficiency and the availability of wind energy and solar energy in the region. Semarang, Indonesia.
.

Index Terms— hydrogen energy, alkaline water electrolysis, renewable energy, solar panel, wind turbine, HHO generator, efficiency.

1 Introduction

The development of clean energy is a vital method in the fight against climate change and limiting the detrimental effects of climate change itself. Nowadays, the fulfillment of energy is still supported by fossil-based sources that have a negative impact on the environment. According to the international energy agency, the world's electricity demand will increase by 70% from 2014 to 2040 Moreover, Final Energy Use will jump from 18% to 23% in the same period, mainly driven by economic growth in India, China, Africa, the Middle East and Southeast Asia [1]. Renewable energy sources accounted for 23% of global electricity supply in 2014, and this percentage is predicted to increase to 58% by 2040 [2].

The problem that is commonly found in the utilization of renewable energy such as solar energy and wind energy sources is the intermittent availability of energy sources, so there will be a mismatch between energy supply and demand. Therefore, storage media is a mandatory part of overcoming this problem. Hydrogen is promoted as an alternative energy storage medium due to its good energy content. 95% of the world's hydrogen production still depends on fossil-based processes [3]. The most commonly used non-fossil-based hydrogen gas production method today is electrolysis using solar panels [4]. The performance of solar panels is very dependent on climatic conditions [5], so it needs to be combined with other energy sources. such as wind energy, to be able to supply power in the required quality[6].

From this description, this research was carried out involving a combination of energy sources based on wind turbines and solar panels by utilizing a water electrolysis system to produce hydrogen as a storage medium for the resulting electrical energy. The purpose of this study is to determine the ability of a combination system based on wind and solar energy using water electrolysis cells to produce hydrogen as an energy storage medium, as well as the potential of solar energy and wind energy in the Semarang region, Indonesia.

2 Theories and Methodology

2.1. Water Electrolysis for Hydrogen Production

Alkaline water electrolysis (AWE) operates at low temperatures (60–80 °C), with a solution of KOH and/or NaOH as the electrolyte, the electrolyte concentration is approximately 20–30% [7]. In alkaline electrolyzers, nickel materials are used as electrodes. The purity of the hydrogen produced is approximately 99%. Alkaline water electrolyzers have an efficiency of around 50-60%[8]. The disadvantage of alkaline electrolysis is its slow response. Long start-up preparation makes it difficult to adapt alkaline electrolyzers to the variable nature of renewable energy sources[9]. The illustration of alkaline water electrolysis working principle can be seen in Fig.2.1.

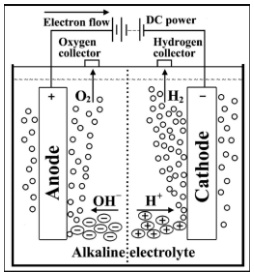

Fig. 2.1. Alkaline water Electrolysis[10]

- *Faisal Rahman is currently pursuing master's degree program in mechanical engineering at Diponegoro University, Indonesia. E-mail: faisal.rahman26@gmail.com*
- *M.S.K. Tony Suryo Utomo is a lecturer and researcher in mechanical engineering department, Diponegoro University, Indonesia. E-mail: msktonysu1971@gmail.com, Corresponding Author.*
- *Berkah fajar T.K. is a professor in mechanical engineering department, Diponegoro University, Indonesia. E-mail: fajarberkah10@gmail.com*

2.2. Thermodynamic Model of Water Electrolysis

Using thermodynamics, the basis of the definition of the driving forces behind the transport phenomena in electrolysis can be determined and can lead to a description of the properties of the electrolyte solution. The following is a brief description of the thermodynamics of low temperature electrochemical reactors used in electrolysis processes.

The total enthalpy change for the electrolysis of water is the enthalpy change between the products (H_2 and O_2) and the reactants (H_2O). The same is true for the change in entropy. The change in Gibbs energy is expressed as

$$\Delta G = \Delta H - T\Delta S \quad (1)$$

Gibbs energy is the amount of energy required for a reversible electrolysis process. The standard Gibbs energy for the water splitting reaction is ΔG = 237 kJ mol^{-1} [11]. Faraday's law relates the electrical energy required for the electrolytic reaction of water to the rate of chemical conversion in a molar quantity. The electrical energy for a reversible electrochemical process or reversible cell voltage is expressed

$$U_{rev} = \frac{\Delta G}{zF} \quad (2)$$

The total amount of energy required for the electrolysis process is equivalent to the change in enthalpy ΔH. From equation (1), it can be seen that ΔG involves thermal irreversibility TΔS, which in a reversible process is equal to the heat requirement. The standard enthalpy for the process of separating water through electrolysis is ΔH = 286 kJ mol^{-1} [4]. From this, we can determine the thermoneutral voltage of the electrolytic cell, which is expressed as follows:

$$U_{tn} = \frac{\Delta H}{zF} \quad (3)$$

Under standard conditions, U_{rev} = 1.229 V and U_{tn} = 1.482 V [20], however, will change with temperature and pressure. In the applicable temperature range, the U_{rev} value decreases with increasing temperature, for example, the U_{rev} value at 80 °C and 1 bar is 1.184 V, while the U_{tn} value remains relatively constant. An increase in pressure will increase the value of U_{rev}; for example, at a temperature of 25 °C and a pressure of 30 bar, the value of U_{rev} becomes 1.295 V and the value of U_{tn} remains constant.

Electrode kinetics can be modeled using the current-voltage relationship (I-U). The basic form of the I-U curve in Fig. 2.2. shows the cell voltage to current density curve at high and low operating temperatures for this type of alkaline water electrolyzer. As can be seen, the difference between the two I-U curves is mainly due to the dependence of the overvoltage on the operating temperature.

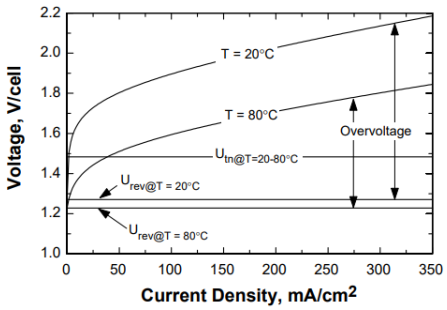

Fig. 2.2 AWE Electrolysis I-U Curve [4]

To find out the amount of gas produced from electrolysis, the ideal gas equation can be used as follows:

$$PV = nRT \quad (4)$$

$$n = \frac{PV}{RT} \quad (5)$$

$$m = \frac{PVMr}{RT} \quad (6)$$

If the electrolyzer does not use a separator, so that the produced gas is a mixture of hydrogen and oxygen gas (HHO), then the mass of each hydrogen and oxygen gas can be obtained using the principle of Dalton's law in the ideal gas equation, where the pressure value is the partial pressure of each gas and the value of the constant R is the specific constant of each gas by first calculating the mole fractions of hydrogen and oxygen gases. As in the following equations:

$$f.O2 = \frac{n_{O2}}{n_{total}} = \frac{1}{3} \quad (7)$$

$$f.H2 = \frac{n_{H2}}{n_{total}} = \frac{2}{3} \quad (8)$$

The partial pressure and constant R of each gas can be determined as in the following equations:

$$P_{O2} = \frac{1}{3} P_{gas\ total} \quad (9)$$

$$R_{O2} = \frac{\mathcal{R}}{M_{O2}} \quad (10)$$

$$P_{H2} = \frac{2}{3} P_{gas\ total} \quad (11)$$

$$R_{H2} = \frac{\mathcal{R}}{M_{H2}} \quad (12)$$

Using the partial pressure and specific gas constant values, the ideal gas equation can be written as follows:

$$P_{O2}V = m_{02}R_{O2}T \quad (13)$$

$$P_{H2}V = m_{H2}R_{H2}T \quad (14)$$

The thermal efficiency of electrolysis can be defined as the ratio between the output in the form of energy content in hydrogen and the input energy as in the following equation [12]:

$$\eta_{elektroliser} = \frac{E\ H_2}{\Delta E} \quad (15)$$

By using the electric power equation for ΔE, and the amount of energy in hydrogen gas is the High Heating Value (HHV) of 141.8 MJ/kg or 283.8 kJ/mol, the equation can be written as follows:

$$\eta_{elektroliser} = \frac{HHV_{H_2}}{\Delta E} = \frac{283{,}8\ (kJ/mol) \times nH_2\ (mol)}{Vit(kJ)} \quad (16)$$

HHV is used with the assumption that hydrogen will later be utilized in a fuel cell where the chemical reaction process will produce water in liquid phase as in a Proton Exchange Membrane type fuel cell where the optimum operating conditions for the fuel cell are at a pressure of 3-4 bar at a temperature of 60-120 °C [13][14], where in this condition the water that is produced is in the liquid phase.

2.3. Wind Energy

Energy takes many forms, each with its own characteristics and qualities. The quality of energy can be interpreted by its capacity or ability to change from one form to another [15]. Wind energy is categorized as "ordered energy". Because the energy that can be utilized is the kinetic energy by using a wind turbine. Analytically, the energy that is utilized from the wind is the magnitude of the change in the kinetic energy of the wind. If it is assumed that kinetic energy can be fully utilized, and the final velocity of the wind after passing through the turbine is zero, the amount of wind power can be expressed mathematically by the following equations [16]:

$$Ek = \frac{1}{2}mv^2 \quad (17)$$

$$\dot{m} = \rho v A \quad (18)$$

$$P_{wind} = \frac{1}{2}\rho A v^3 \quad (19)$$

2.4. Solar Energy

The greatest source of energy available to humans is the sun. The photovoltaic system is one method of harvesting solar energy. Photovoltaic system energy conversion is an energy conversion in one step, which is to produce electrical energy from solar energy. The photovoltaic system uses a semiconductor material with the p-n junction principle, which can conduct electric current when receiving energy in the form of photons. An illustration of the working principle of a photovoltaic cell can be seen in Fig. 2.3.

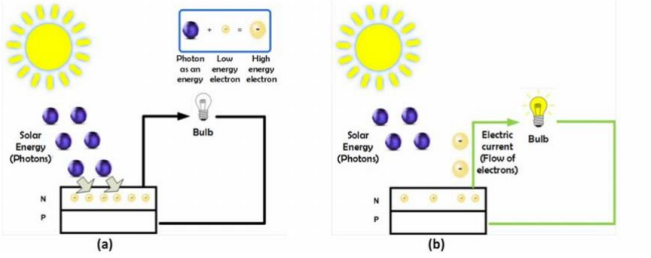

Fig. 2.3 Photovoltaic Working Principle [17]

The performance of a PV panel can be characterized by the I-V characteristic curve, namely the current and voltage curve of the PV panel in the case of solar irradiation of 1000 W/m² at a panel operating temperature of 25 °C. An example is the I-V curve in Fig. 2.4. The three points on the I-V curve that are important in defining the performance of a PV panel; Short-circuit current I_{SC}; this parameter shows the maximum current generated by the pv panel when the load is zero or the voltage value is zero (V = 0); open circuit voltage V_{OC}, which shows the maximum voltage that can be achieved by the pv panel under conditions where the load is infinite or the current is zero (I = 0). The power curve is the product of the current and voltage generated by the solar panel.

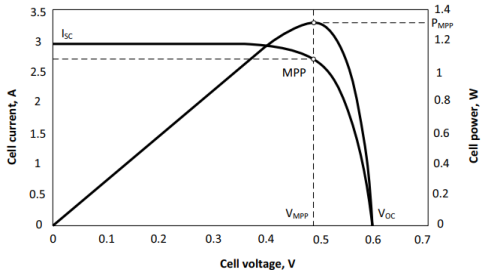

Fig. 2.4. Solar Panel Characteristic Curve [18]

2.5. Experimental Setup

This study used alkaline water electrolysis type with SS316L stainless steel as the material for the electrode, referring to a previous study by El Soly [8] where SS316L material was used to compare electrolysis in dry cells and wet cells. In addition, SS316 material was also used by Olivares [19] in his research, namely to see the hydrogen evolution reaction in the electrolysis process. The shape of the electrode is a flat plate. The dimensions of the electrolyzer can be seen in Table 2.1, and the schematic of the electrolyzer circuit is shown in Fig. 2.5.

Table 2.1. Electrolyzer Specification

Specification	Value
Cell volume	1,4 L
Electrode dimension	70 x 70 x 1,5 mm
Amount of electrode	10
Electrode material	SS316
Electrolyte	NaOH
Electrolyte concentration	25%wt

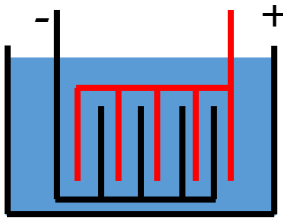

Fig. 2.5. Electrolyzer schematic

The detailed specifications of the turbine and solar panels used are shown in Fig. 2.6., Table 2.2, Table 2.3, and Fig. 2.7. The experimental setup can be seen in Fig.2.8.

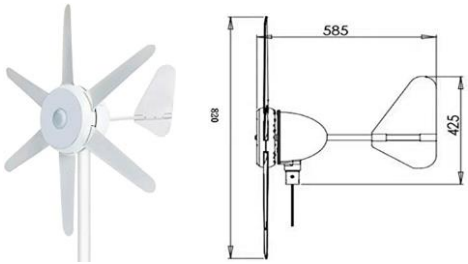

Fig. 2.6. Wind Turbine

Table 2.2 Wind Turbine Specification

Specification	Value
Blade	6
Starting wind speed	1 m/s
Rated wind speed	12 m/s
Output Voltage	12V
Maximum Power	300W

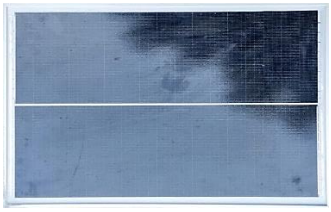

Fig. 2.7 Solar Panel

Table. 2.3. Solar Panel Specification

Specification	Value
Dimension	350 × 530 × 25 mm
Maximum Power point	30 W
Voltage at Pmax (V_{mp})	18.4 V
Current at Pmax (I_{mp})	2.72 A
Open-Circuit Voltage (V_{oc})	22.6 V
Short-Circuit Current	2.94 A

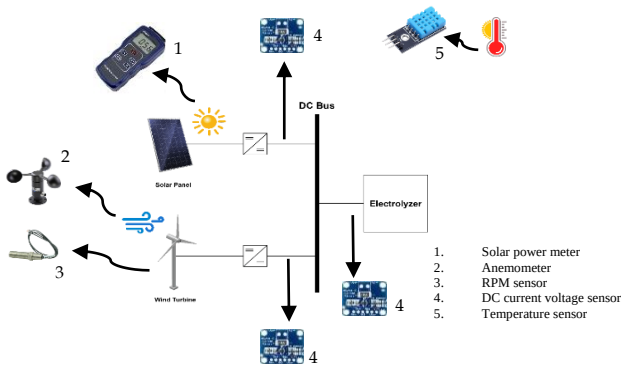

Fig. 2.8. Experimental setup

The amount of gas is measured using a measuring cylinder, as shown in Fig. 2.9. and the gas pressure is calculated by equation 20.

$$P_{gas} = P_{atm} - \rho g h_{air} \quad (20)$$

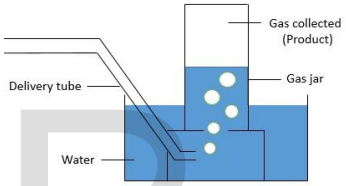

Fig. 2.9. Gas Measurement Setup

The amount of energy contained in the gas can be calculated using the following equation:

$$E_{H_2}(kJ) = Mass\ H_2(kg) \times HHV\ H_2\ (kj/kg) \quad (21)$$

System efficiency is obtained from the ratio between the energy contained in the hydrogen and the input energy, which is wind energy obtained from equation 19, and the theoretical maximum energy that can be produced by solar panels with irradiation as measured using a solar power meter. System efficiency is written in equation 22

$$\eta_{th} = \frac{E_{out}}{E_{in}} = \frac{E_{H_2}}{E_{wind}+E_{solar}} \times 100\% \quad (22)$$

3 Result and Discussion

3.1. Solar Panel Measurement Result

Electrolysis experiment using wind turbine and solar panel, was carried out for four days from 09:00 to 16:00. The results of measurements of solar irradiation are shown in Fig.3.1, and the average value of irradiation and the amount of energy produced by the solar panels are shown in Table 3.1.

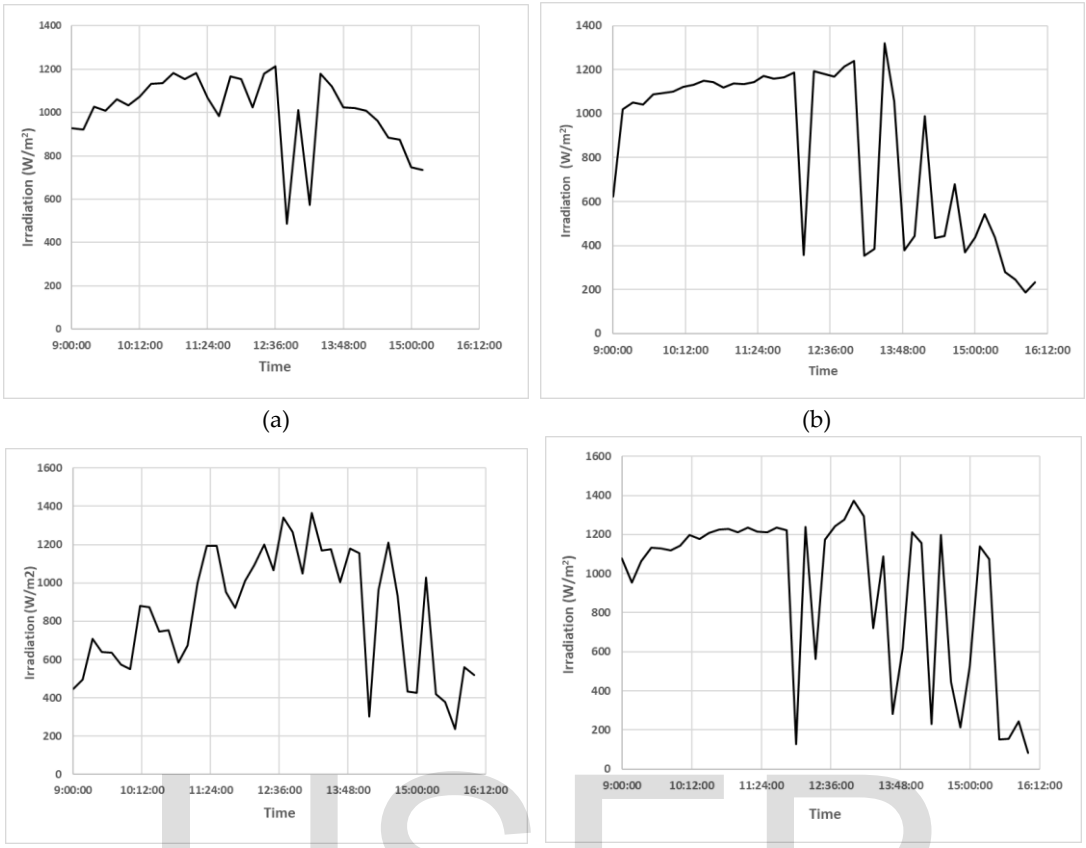

Fig 3.1 Solar Irradiation, (a) day-1, (b) day-2, (c) day-3, (d) day-4.

Table 3.1 Average Irradiation, Total Theoritical Maximum Solar Energy, Actual Electrical Energy

Day	Average Irradiation (w/m^2)	Total Theoritical Maximum Solar Energy (J)	Actual Electrical Energy (J)
1	1007,906	574361.424	72576.93531
2	845,332	647308.3344	84369.7805
3	843,337	645780.408	87556.225
4	926.611	708781.372	97657.88

From table 3.1 the average value of solar irradiation on the experiment date ranged from 843.332 W/m2 to the highest on the first day of 1007.906 W/m2. Table 3.1 also shows a comparison between the theoretical maximum energy that can be generated and the actual electrical energy generated by solar panels. Solar panels only convert about 13% of the theoretical maximum energy that can be generated. Cloud activity caused massive fluctuations, as shown in Fig. 3.1.

Even though fluctuations occur, the voltage from the solar panels remains above the U_{tn} value so that the solar panels can continue to supply electricity for the electrolysis process. The measurements results of voltage, current, and electric power of solar panels are shown in Fig. 3.2., 3.3. and 3.4. below.

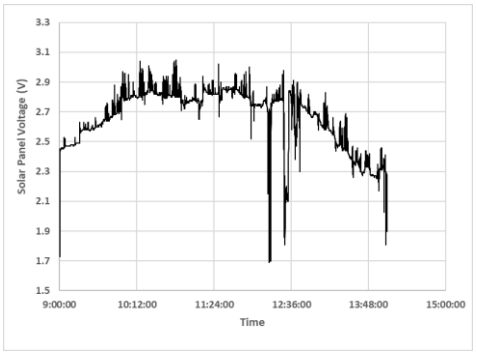

(a)

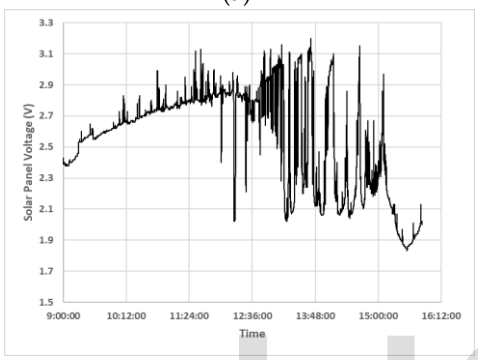

(b)

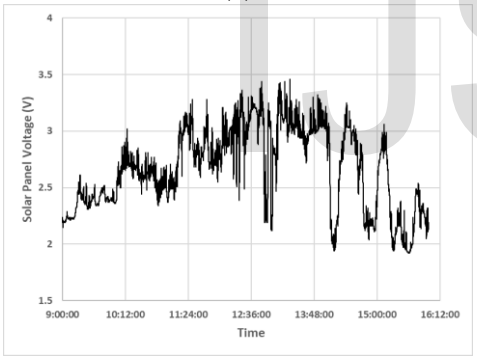

(c)

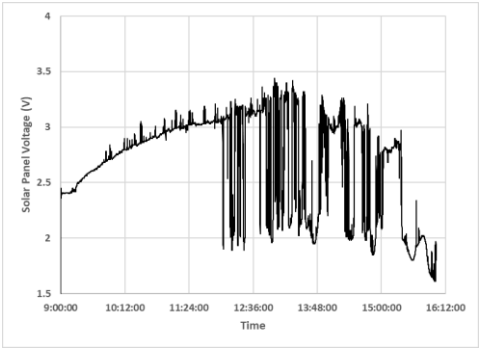

(d)

Fig 3.2 Solar Panel Voltage, (a) day-1, (b) day-2, (c) day-3, (d) day-4.

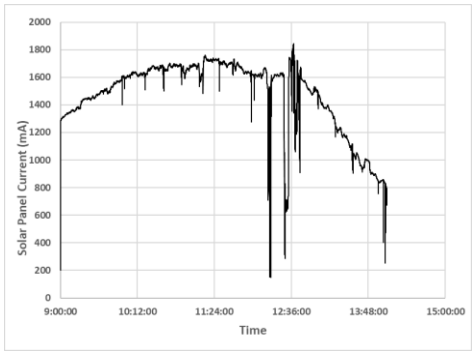

(a)

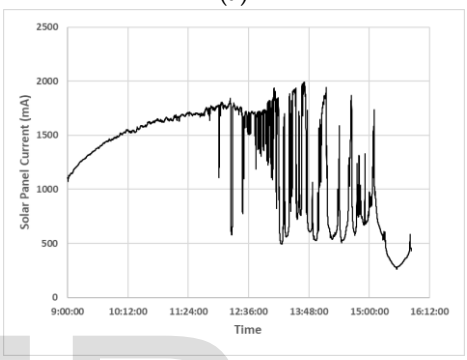

(b)

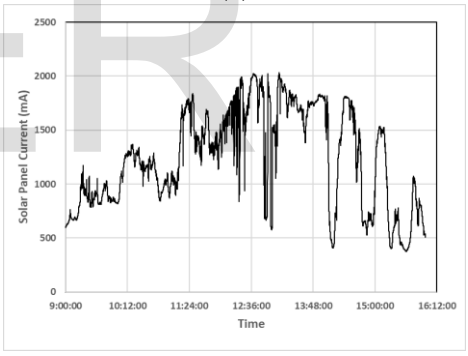

(c)

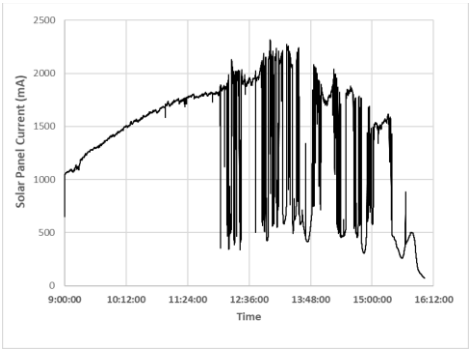

(d)

Fig 3.3 Solar Panel Current, (a) day-1, (b) day-2, (c) day-3, (d) day-4.

From the experimental results, the power output of the solar panel looks quite far from the specifications, where the solar panel can supply 30 watts of power under standard test conditions. The resulting voltage is also quite far from the Vmp value, which is 18V. This is caused by loading that is not at the optimum point. The output power of the solar panel is greatly influenced by the load resistance R_L, in this case, the electrolyzer. The effect of load resistance on power output has also been tested by Ouedagardo [20] who tested solar panels with variable loads. And it can be seen that the power generated will be maximum at a certain load resistance, as shown in Fig.3.4.

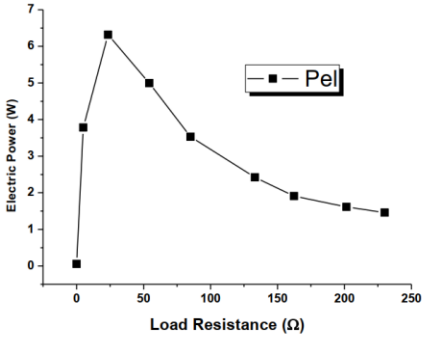

Fig. 3.4. output of solar panel electric power at various resistance loads [46]

This loss of power is caused by two parasitic parameters, namely shunt resistance (R_{sh}) and series resistance (R_s). Shunt resistance is defined as the leakage current [21]. The effect of the shunt resistance will also be strengthened in weak irradiation conditions. Shunt resistance can be calculated using equation 23 [22][23].

$$R_{sh} = \frac{V}{I_{sc}-I} \quad (23)$$

Where V is the circuit voltage, and I is the current flowing in the circuit. The second parasitic parameter is series resistance. Series resistance is the resistance that occurs in the contact between solar panel materials. series resistance can decrease the fill factor, and at large values, it will decrease Isc. Series resistance can be calculated by equation 23 [24] and the equivalent circuit of Rs and Rsh is shown in Fig. 3.5.

$$R_s = \frac{V_{oc}-V}{I} \quad (23)$$

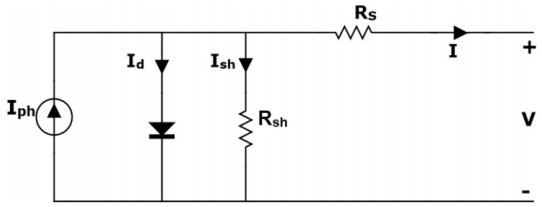

Fig. 3.5. Equivalent Circuit of Solar Panel [48]

Ideally, Rsh should be equal to ∞ and Rs should be equal to 0. The effect of load resistance on these two parameters is shown in Fig. 3.6.

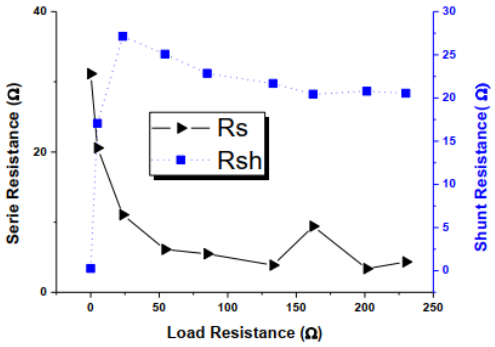

Fig 3.6 R_{sh} and R_s at various load resistance

Comparing Fig. 3.4. with Fig. 3.6., it can be seen that the maximum power output is shown to occur when the Rsh value is high and the Rs value is low. As for the values of Rsh and Rs in this experiment, the results are shown in Table 3.2., where the value of Rs is very large and the value of Rsh is very small, which of course will result in non-optimal solar panel performance.

Table 3.2. R_{sh} and R_s value from experiment

Day	Shunt Resistance R_{sh} (Ω)	Series resistance R_s (Ω)
1	1,880	14,572
2	1,722	20,665
3	1,762	19,227
4	1,994	23,831

3.2. Wind Turbine Measurment Result

Data on wind speed and turbine rotation are shown in Fig. 3.7. and 3.8. as follows, and data on wind energy, such as average wind speed, maximum speed, total wind energy, and electrical energy from wind turbine, can be seen in Table 3.3.

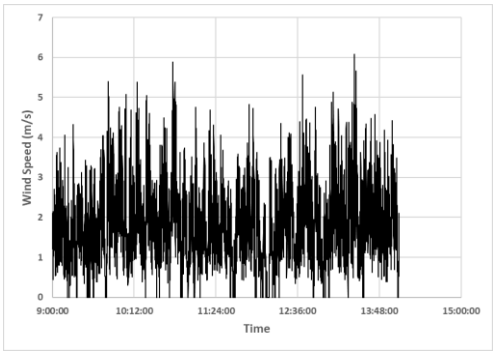

(a)

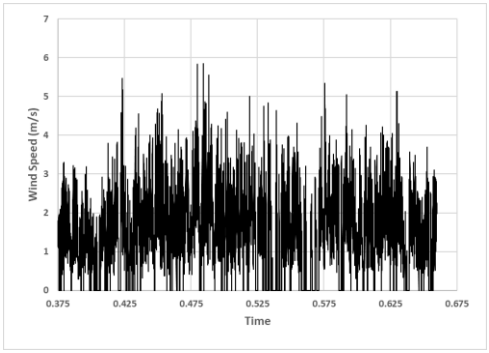

(b)

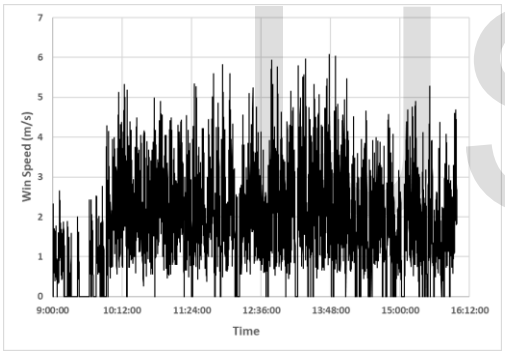

(c)

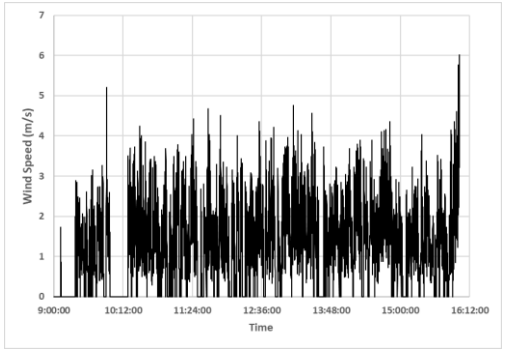

(d)

Fig. 3.7. Wind Speed, (a) day-1, (b) day-2, (c) day-3, (d) day-4.

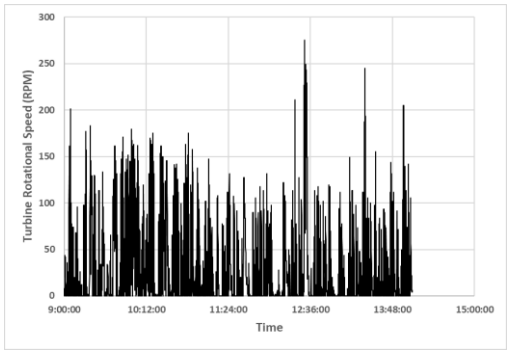

(a)

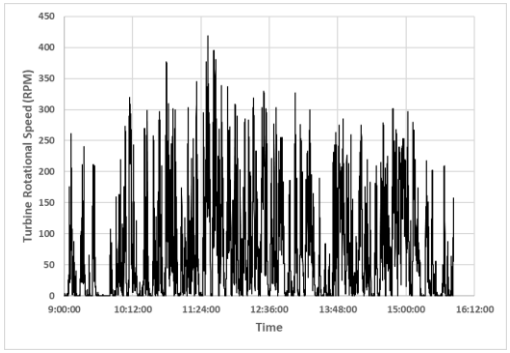

(b)

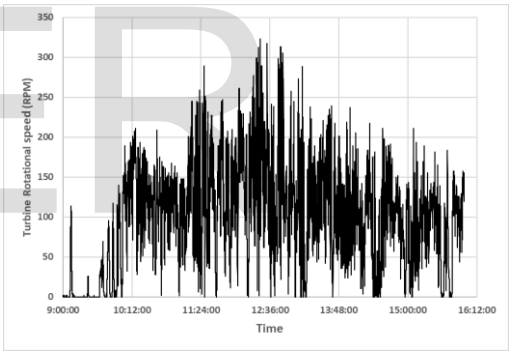

(c)

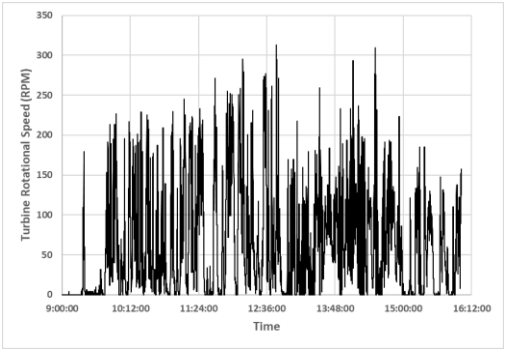

(d)

Fig. 3.8. Turbine Rotational Speed, (a) day-1, (b) day-2, (c) day-3, (d) day-4.

The poor continuity of the wind speed causes an unstable supply of electrical energy. Unlike the solar panel, the voltage from wind turbine cannot remain above the the U_{tn} voltage. Measurements of voltage, current, and wind turbine power are shown in Fig. 3.9., 3.10. and 3.11.
The largest amount of electrical energy is generated on the third day, which is 4216,485 J. Looking at the wind speed data, it can be seen that the wind speed on the third day has better continuity compared to other days, and also on the third day the average wind speed reaches the highest value compared to other days, so that the turbine can supply more electricity.

Table 3.3. average wind speed, maximum wind speed, total value of wind energy and turbine electricity

Day	Average Wind Speed (m/s)	Max. wind speed (m/s)	Wind Enegy Total (J)	Electrical Energy Total (J)
1	1.785	6.08	25487,319	1402.771
2	1.544	5.85	22290.002	1211.622
3	1.806	6.07	74334.762	4216.485
4	1.268	6.01	25282.697	1087.629

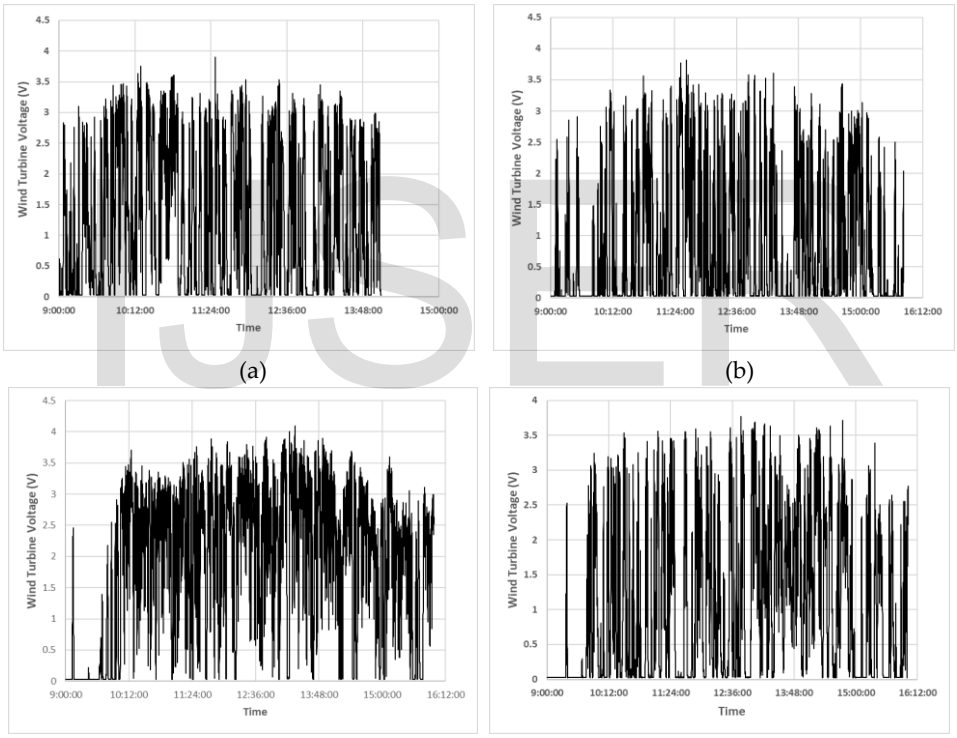

(a) (b)

(c) (d)

Fig. 3.9. Wind Turbine Voltage, (a) day-1, (b) day-2, (c) day-3, (d) day-4.

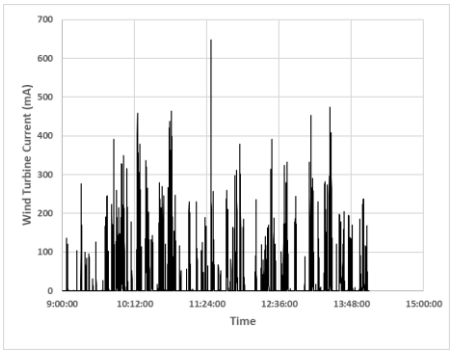

(a)

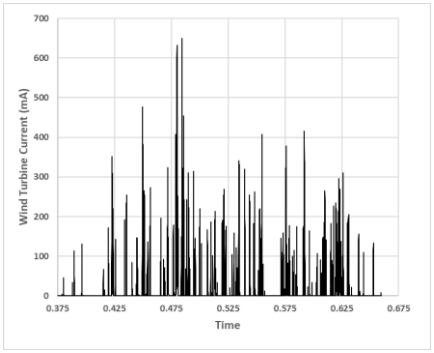

(b)

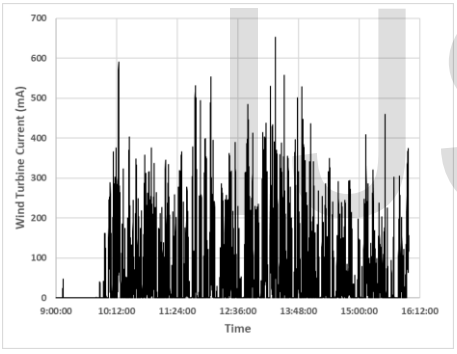

(d)

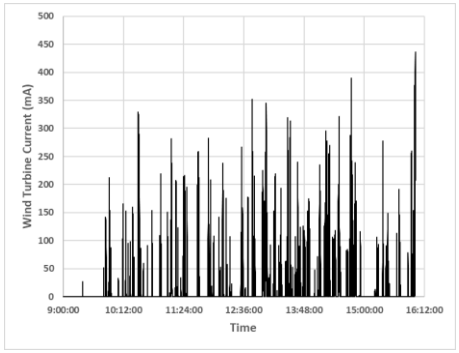

(d)

Fig. 3.10. Wind Turbnine Electric Current, (a) day-1, (b) day-2, (c) day-3, (d) day-4.

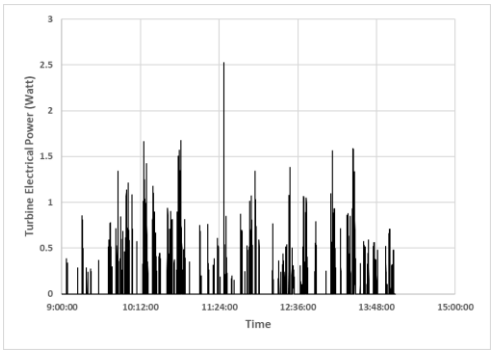

(a)

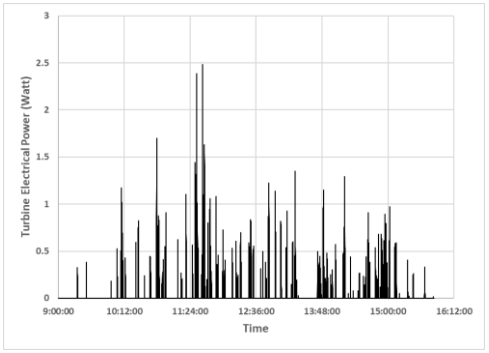

(b)

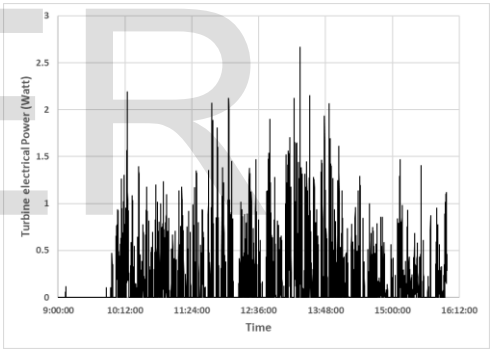

(c)

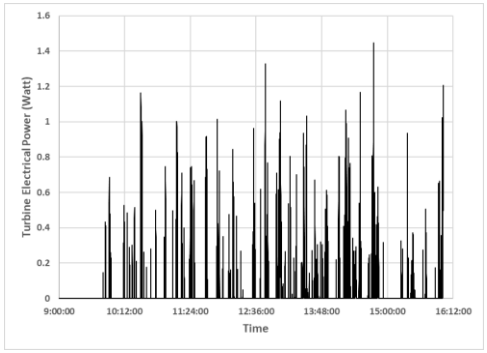

(d)

Fig. 3.11. Wind Turbine Electrical Power, (a) day-1, (b) day-2, (c) day-3, (d) day-4.

3.3. Combination system Result

The measurement results show that more than 95% of the electricity is supplied by the solar panel, and the wind turbine only contributes a small percentage of total electrical energy, as shown in table 3.4. Even so, the use of these two sources can still increase the output power compared to using only one of them. The test results of electrical output can be seen in Fig. 3.11., 3.12, and 3.13. as follows:

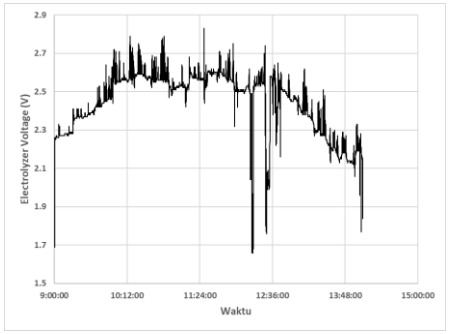

(a)

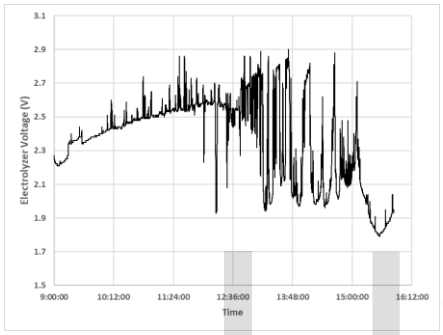

(b)

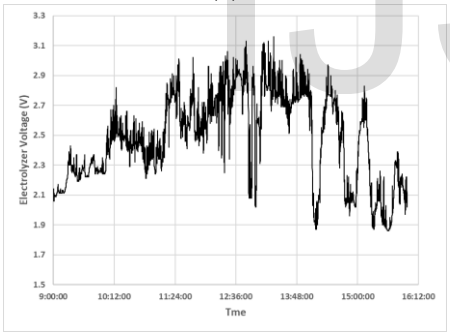

(c)

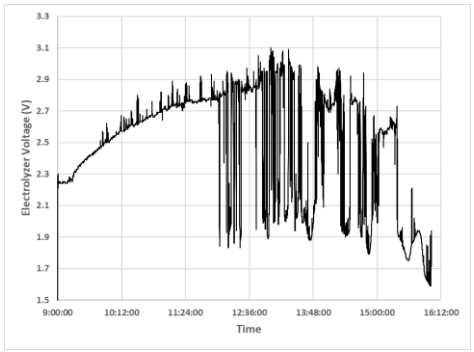

(d)

Fig. 3.12. Electrolyzer Voltage, (a) day-1, (b) day-2, (c) day-3, (d) day-4.

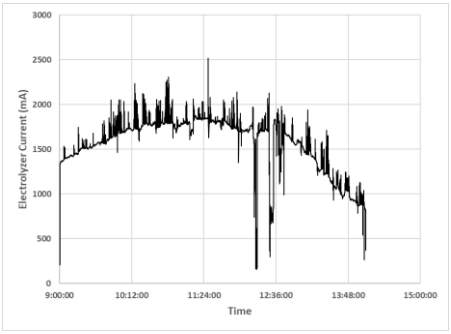

(a)

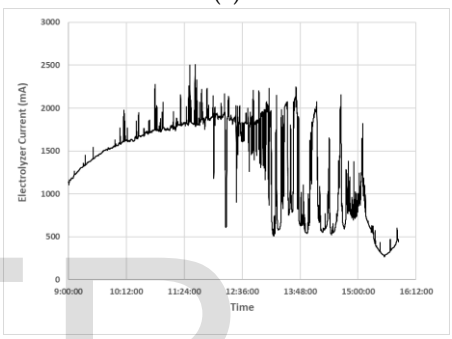

(b)

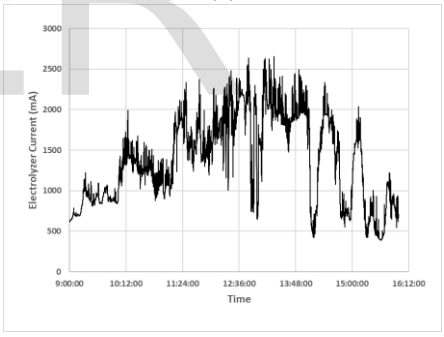

(c)

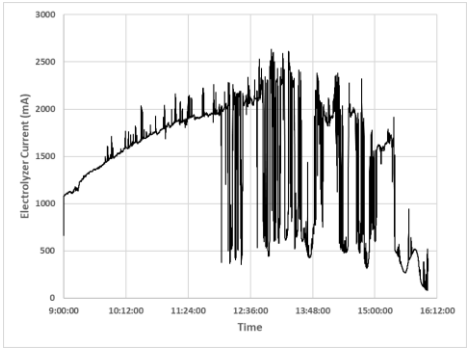

(d)

Fig 3.13. Electrolyzer Current, (a) day-1, (b) day-2, (c) day-3, (d) day-4.

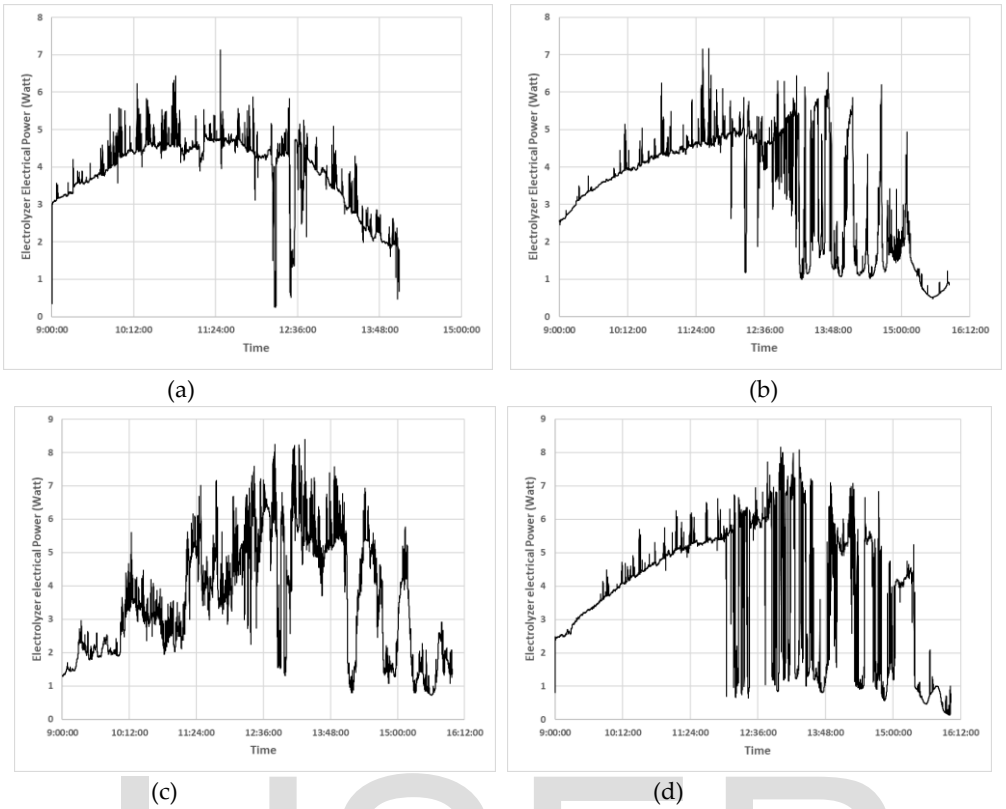

Fig 3.14. Electrolyzer Electrical Power, (a) day-1, (b) day-2, (c) day-3, (d) day-4.

Tabel 3.4. Combination System Result

Day	Electrolyzer electrical energy (J)	Solar panel electrical energy (J)	Wind turbine electrical energy (J)	Total electrical energy (J)	% Turbine electrical energy supply	% Solar panel electrical energy supply	% Losses in circuit
1	71512.006	72576.935	1402.77	73979.71	1.896	98.104	3.336
2	83064.902	84369.781	1211.622	85581.403	1.416	98.584	2.9405
3	89829.670	87556.225	4216.485	91772.709	4.595	95.406	2.117
4	96589.033	97657.880	1087.629	98745.509	1.101	98.89	2.184

.

3.4. Electrolyzer Measurement Result

In this experiment, the product produced by the electrolyzer is in the form of HHO gas. The HHO gas product produced by the electrolyzer was measured every 15 minutes during the test. The amount of HHO gas produced every 15 minutes are presented in Figures 3.15., The trend of HHO gas production is strongly influenced by the performance of solar panels. From the measured gas volume, its mass can then be calculated, and then the energy content in hydrogen gas can be obtained by using equations 21.

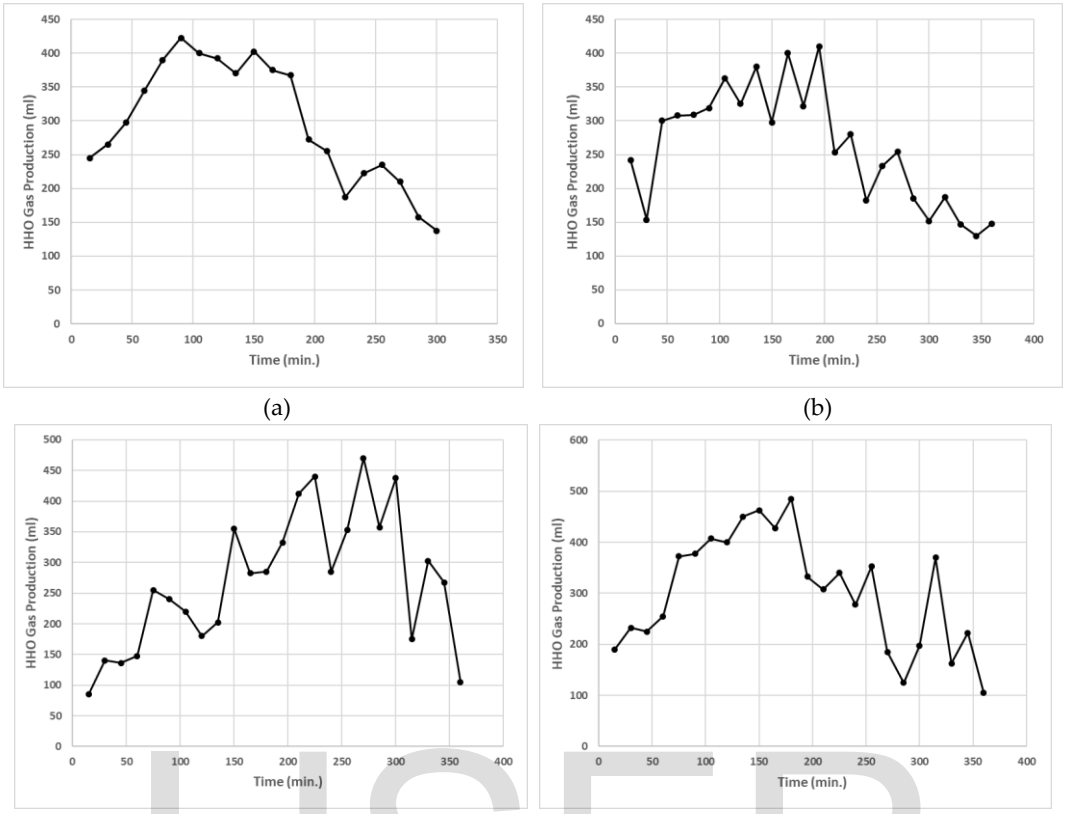

Fig. 3.15. HHO Gas Produced, (a) day-1, (b) day-2, (c) day-3, (d) day-4.

Table 3.5. Electrolyzer calculation result.

Day	HHO gas Production rate (ml/hr)	HHO gas Total (ml)	Hydrogen Energy (j)	Electrolyzer electricity input (j)	Electrolyzer efficiency (%)
1	1190	5950	44946.803	71512.006	62.414
2	1046,833	6281	47426.461	83064.902	61.409
3	1077,583	6465.5	48829.855	89829.670	58.184
4	1210,417	7262.5	54790.346	96589.033	60.622

From table 3.5 the electrolyzer made can produce HHO gas with an average rate during the test of 1131,208 ml/hour and has an average efficiency of 60.657%. The resulting efficiency value has shown a fairly good number. The resulting efficiency is also in accordance with the results obtained by El Soly [8], in his research on the electrolysis of dry cells and wet cells using stainless steel electrodes. The study found that the efficiency values varied between 45% to 75%. The resulting overall system efficiency can be seen in Table 3.6.

The efficiency of the system is calculated by equation 27, where the total energy is the sum of the solar energy and the theoretical maximum energy of the solar panels. The average efficiency of an alkaline water electrolysis system with a combination system of solar panels and wind turbine is 6.843%. The low resulting efficiency is due to inadequately performing solar panels, as explained in previous section.

Table 3.6 System Efficiency

Day	Total Energy Input (J)	Hydrogen Energy (J)	System Efficiency (%)
1	743439.1	44946.803	6.046
2	669598.337	47426.461	7.083
3	720115.17	48829.855	6.781
4	734064.069	54790.346	7.464

4 Conclusion

The solar irradiation measurement shows the average irradiations for each day were 1007,906 W/ m², 845,332 W/ m², 843,337 W/ m², and 926,611 W/m². The average wind Speeds were 1.785 m/s, 1.544 m/s, 1.806 m/s, and 1.268 m/s. During the test, the amounts of HHO gas produced were 5950 ml, 6281 ml, 6465.5 ml, and 7262.5 ml, with an average flow rate of 1131,208 ml/hour. The efficiency values of the electrolyzer for each day were obtained at 62.414%, 61.409%, 58.184%, and 60.622%, with an average efficiency of 60.657%. The system efficiencies for each day are 6.046%, 7.083%, 6.781%, and 7.464%, with an average of 6.843%. The low system efficiency is caused by a mismatch between the load resistance (electrolyzer) and the main source (solar panels), which results in shunt resistance and series resistance values that are not ideal. This causes a decrease in the electrical power output of the solar panels. More than 95% of the electricity for the electrolyzer is supplied by solar panels, so optimizing the working conditions of the solar panels will determine the results of electrolysis. The low involvement of wind turbines in supplying power is caused by the inadequate availability of wind energy sources—low speed and poor continuity. The energy source that gives optimistic results for an alternative energy source in the Semarang area, especially Tembalang, is solar energy. On the other hand, wind energy has not given as good results as solar energy.

5 Recommendation

According to the results of the analysis and conclusions stated in the previous section, this research is still very feasible to be developed by optimizing the components, namely solar panels, wind turbines, and electrolyzers. Solar panels can be optimized by adding the MPPT (Maximum Power Point Tracking) algorithm to keep them working at their maximum power points. Then it is necessary to adjust the load resistance connected to the solar panel to minimize losses due to shunt resistance and series resistance on the solar panel. In addition, solar panels can also be modified with a series connection to increase the current strength so as to accelerate electron exchange and increase the current density, which will affect gas production. Then, for wind turbines, low wind speed turbine specifications such as the Savonius turbine can be used so that the wind energy conversion process can be maximized. It can also be improved from the electrolyzer side by changing the electrode material, the type and concentration of the electrolyte, the configuration and geometry of the electrode, and the electrode's size, which will also boost gas production.

6 References

[1] International Energy Agency, "Climate Change and the 450 Scenario. The door is closing, but when will we be 'Locked-in'?," *World Energy Outlook*, pp. 1–666, 2012.

[2] G. Maggio, A. Nicita, and G. Squadrito, "How the hydrogen production from RES could change energy and fuel markets: A review of recent literature," *Int. J. Hydrogen Energy*, vol. 44, no. 23, pp. 11371–11384, 2019, doi: 10.1016/j.ijhydene.2019.03.121.

[3] S. Banerjee, M. N. Musa, and A. B. Jaafar, "Economic assessment and prospect of hydrogen generated by OTEC as future fuel," *Int. J. Hydrogen Energy*, vol. 42, no. 1, pp. 26–37, 2017, doi: 10.1016/j.ijhydene.2016.11.115.

[4] Ø. Ulleberg, "Modeling of advanced alkaline electrolyzers a system," *Hydrog. Energy*, vol. 28, pp. 21–33, 2003, [Online]. Available: http://ac.els-cdn.com/S0360319902000332/1-s2.0-S0360319902000332-main.pdf?_tid=9de625b8-a749-11e2-af8d-00000aab0f6b&acdnat=1366194721_e2bd5a3ec87dd1ed6fb5af4c9b55380e

[5] L. Wang and C. Singh, "PSO-Based Multidisciplinary Design of A Hybrid Power Generation System With Statistical Models of Wind Speed and Solar Insolation," 2007, pp. 1–6. doi: 10.1109/PEDES.2006.344273.

[6] B. N. Prashanth, R. Pramod, and G. B. V. Kumar, "Design and Development of Hybrid Wind and Solar Energy System for Power Generation," *Mater. Today Proc.*, vol. 5, no. 5, pp. 11415–11422, 2018, doi: 10.1016/j.matpr.2018.02.109.

[7] I. M. Sakr, S. El-kom, A. A. Balabel, and K. A. Ibrahim, "Experimental Investigation of the Operating Parameters Affecting Hydrogen Production Process through Alkaline Water Electrolysis," no. August 2015, 2010, doi: 10.5383/ijtee.02.02.009.

[8] A. K. El Soly, M. A. El Kady, A. El, F. Farrag, and M. S. Gad, "ScienceDirect Comparative experimental investigation of oxyhydrogen (HHO) production rate using dry and wet cells," *Int. J. Hydrogen Energy*, vol. 46, no. 24, pp. 12639–12653, 2021, doi: 10.1016/j.ijhydene.2021.01.110.

[9] G. Gahleitner, "Hydrogen from renewable electricity : An international review of power-to-gas pilot plants for stationary applications," *Int. J. Hydrogen Energy*, vol. 38, no. 5, pp. 2039–2061, 2012, doi: 10.1016/j.ijhydene.2012.12.010.

[10] R. Ziazi, K. Mohammadi, and N. Goudarzi, "Techno-economic assessment of utilizing wind energy for hydrogen production through electrolysis," *Am. Soc. Mech. Eng. Power Div. POWER*, vol. 2, no. March 2019, 2017, doi: 10.1115/POWER-ICOPE2017-3675.

[11] S. Anwar, F. Khan, Y. Zhang, and A. Djire, "Recent

development in electrocatalysts for hydrogen production through water electrolysis," *Int. J. Hydrogen Energy*, vol. 46, no. 63, pp. 32284–32317, 2021, doi: 10.1016/j.ijhydene.2021.06.191.

[12] K. Zeng and D. Zhang, "Recent progress in alkaline water electrolysis for hydrogen production and applications," *Prog. Energy Combust. Sci.*, vol. 36, no. 3, pp. 307–326, 2010, doi: 10.1016/j.pecs.2009.11.002.

[13] J. Hoeflinger and P. Hofmann, "Air mass flow and pressure optimisation of a PEM fuel cell range extender system," *Int. J. Hydrogen Energy*, vol. 45, no. 53, pp. 29246–29258, 2020, doi: 10.1016/j.ijhydene.2020.07.176.

[14] N. Ahmadi, A. Dadvand, S. Rezazadeh, and I. Mirzaee, "Analysis of the operating pressure and GDL geometrical configuration effect on PEM fuel cell performance," *J. Brazilian Soc. Mech. Sci. Eng.*, vol. 38, no. 8, pp. 2311–2325, 2016, doi: 10.1007/s40430-016-0548-0.

[15] T. . Kotas, *The Exergy Method of Thermal Plant Analysis.*, Fourth ed. London: Krieger Publishing Company, 1995.

[16] Y. A. Çengel, M. A. Boles, and M. Kanoglu, *Thermodynamics: An Engineering Approach*. McGraw-Hill Education, 2018. [Online]. Available: https://books.google.co.id/books?id=lN9JswEACAAJ

[17] S. Abdelhady, M. S. Abd-Elhady, and M. M. Fouad, "An Understanding of the Operation of Silicon Photovoltaic Panels," *Energy Procedia*, vol. 113, pp. 466–475, 2017, doi: 10.1016/j.egypro.2017.04.041.

[18] S. Makhija, A. Khatwani, M. F. Khan, V. Goel, and M. M. Roja, "Design \& implementation of an automated dual-axis solar tracker with data-logging," *2017 Int. Conf. Inven. Syst. Control*, pp. 1–4, 2017.

[19] J. M. Olivares-Ramírez, M. L. Campos-Cornelio, J. Uribe Godínez, E. Borja-Arco, and R. H. Castellanos, "Studies on the hydrogen evolution reaction on different stainless steels," *Int. J. Hydrogen Energy*, vol. 32, no. 15 SPEC. ISS., pp. 3170–3173, 2007, doi: 10.1016/j.ijhydene.2006.03.017.

[20] A. Ouedraogo *et al.*, "Analysis Of External Load Resistance Influence On The Single-Crystalline Silicon Photovoltaic Module (PV)," *J Fundam Appl Sci*, vol. 2019, no. 2, pp. 663–674, 2019, doi: 10.4314/jfas.v11i2.8.

[21] J. H. Qin, L. Wang, S. S. Yang, and R. Huang, "The effect of solar cell shunt resistance change on the bus voltage ripple in spacecraft power system," *Microelectron. Reliab.*, vol. 88–90, pp. 1047–1050, Sep. 2018, doi: 10.1016/j.microrel.2018.06.095.

[22] C. S. Ruschel, F. P. Gasparin, E. R. Costa, and A. Krenzinger, "Assessment of PV modules shunt resistance dependence on solar irradiance," *Sol. Energy*, vol. 133, pp. 35–43, Aug. 2016, doi: 10.1016/j.solener.2016.03.047.

[23] F. Toure *et al.*, "Influence of Magnetic Field on Electrical Model and Electrical Parameters of a Solar Cell Under Intense Multispectral Illumination Influence of Magnetic Field on Electrical Model and Electrical Parameters of a Solar Cell Under Intense Multispectral Illumi," *Type Double Blind Peer Rev. Int. Res. J. Publ. Glob. Journals Inc*, vol. 12, 2012.

[24] D. U. Combari, I. Zerbo, M. Zoungrana, E. W. Ramde, and D. J. Bathiebo, "Modelling Study of Magnetic Field Effect on the Performance of a Silicon Photovoltaic Module," *Energy Power Eng.*, vol. 09, no. 08, pp. 419–429, 2017, doi: 10.4236/epe.2017.98028.